Research Square

Preprints are preliminary reports that have not undergone peer review.
They should not be considered conclusive, used to inform clinical practice,
or referenced by the media as validated information.

Thermal stress ahead of arrested dyke tips with implications for the reinitiation of dyke propagation

John Browning

j.browning@ucl.ac.uk

University College London

Jorge Cortez

Universidad de La Serena

Research Article

Keywords: Fracture Propagation, Thermo-mechanics, Stalled magmas, Dykes and Inclined Sheets

Posted Date: November 16th, 2026

DOI: https://doi.org/10.21203/rs.3.rs-11480056/v1

License: This work is licensed under a Creative Commons Attribution 4.0 International License.
Read Full License

Additional Declarations: No competing interests reported.

Thermal stress ahead of arrested dyke tips with implications for the reinitiation of dyke propagation

John Browning[1,3*] and Jorge Cortez[2,3]

[1]Department of Earth Sciences, University College London, UK

[2]Department of Mining Engineering, Universidad de La Serena, La Serena, Chile.

[3]Department of Mining Engineering, Pontificia Universidad Católica de Chile, Santiago, Chile

[*]Corresponding author: j.browning@ucl.ac.uk

ABSTRACT

Understanding the movement of magma within the crust is essential for interpreting volcanic unrest signals and ultimately forecasting volcanic eruptions. Magma ascends through the crust by generating pressure-driven fractures at the leading tips of dykes and inclined sheets. The vast majority of studies investigating the mechanics of magma propagation neglect the influence and effect of temperature on the rock surrounding intrusions during emplacement. However, magma can disrupt temperature fields, leading to thermal expansion or contraction of the surrounding host rocks and to the generation of thermal stress and thermal fractures. This study uses a thermo-mechanical approach to investigate thermal stress perturbations around dyke tips and considers how insight from numerical experiments may be utilized to interpret geophysical signatures. Despite limited data

on rock physical properties at elevated temperatures, existing data suggest a non-linear relationship between temperature and thermal expansion/contraction co-efficient. A two-dimensional nonlinear thermo-mechanical transient model was implemented using the finite element method (FEM). Results show that thermal stress in the direction parallel to dyke propagation suppresses tensile stresses predicted by purely elastic models, potentially creating stress conditions that are more favourable for mixed-mode failure involving both tensile and shear components near the dyke tip. The results become particularly salient for magma sheets that become stalled and are given time to heat and alter the surrounding host rocks. In these circumstances, sheets may resume their propagation, following arrest, if the combination of magma pressure and thermal stress overcome the local rock strength.

Keywords: Fracture Propagation, Thermo-mechanics, Stalled magmas, Dykes and Inclined Sheets.

HIGHLIGHTS

- Thermo-mechanical modelling provides insight into the reinitiation of arrested magma paths due to thermal stress.
- Thermal stress parallel to the direction of the dyke propagation suppress tensile stress found in purely elastic models.
- Magma sheet fracture mechanics may change from dilatant crack opening to hybrid shear displacement when temperature considered.

INTRODUCTION

Magma propagates through the crust to feed volcanic eruptions by generating pressure-driven fractures ahead of dykes and inclined sheets (Rubin, 1995). Magma sheets are tabular intrusive bodies that form when the stress conditions at the margin of a magma chamber are sufficiently high to rupture the surrounding rock and form a fracture which the magma then fills (Gudmundsson, 2020). Magma does not always reach the surface but instead can often become arrested at depth (Gudmundsson, 2006). The arrest of magma is controlled by three main mechanisms that are intrinsically related to the properties of the rock surrounding the magma: (1) by generating stress barriers, (2) through elastic mismatch, and (3) Cook-Gordon delamination. Stress barriers occur when the orientation of principal stresses rotate, often at the contact between rock layers with different mechanical properties (Gudmundsson, 2011a). Magma propagates approximately parallel with the maximum principal compressive stress (σ_1). If σ_1 rotates by 90°, the magma sheet may become arrested or deflect into a sill. An elastic mismatch occurs when there is a large difference between the modulus of elasticity of the two rock layers in contact, which can also prevent the propagation of the magma sheet and promote its deflection or arrest as the magnitude of stress may not be sufficiently high in one of the layers to grow the fracture. Finally, Cook-Gordon delamination occurs when the stresses induced at the tip of a sheet delaminate or pull apart the lithological contact between the two layers (Clunes et al. 2021; Gudmundsson 2011a, 2011b) and favours the deflection or arrest of the dyke. Elevated temperature may also play

a role in the distribution of stress around magma sheets (dykes/sills), especially in voluminous and multiple dykes (Figure 1) (Fialko and Rubin, 1999). Since magma emplaces at temperatures exceeding 600°C (Bartlett, 1969; Green et al., 2001) the potential to develop thermal stress within the often significantly cooler surrounding rock is great. However, relatively little work has been done to characterize this effect. In fact, the vast majority of magma propagation models assume the crust to be elastic and with no or little thermal perturbation (e.g. Delaney et al., 1986; Rubin 1995; Gudmundsson, 2011; Rivalta et al., 2015; Healy et al., 2018). The few models that do consider elevated temperatures have focused on determining deformation around large magma bodies, often invoking visco-elasticity (e.g. Gregg et al., 2013; Hickey et al., 2016). Numerical models at this scale show that thermal stresses increase the shear stress around the magma chamber and partially suppress the tensile stress when compared to a purely elastic model (Browning et al., 2021), however, the effect of thermal loads induced during heat exchange at the scale of individual sheets, over the timescales of common unrest periods (Figure 1B) has yet to be quantified. The amount of damage induced by thermal stress (Figure 1C) also depends on rock composition (Daoud et al., 2020) and has consequences for development of thermal haloes (Hofer-Apostolidis et al., 2024). As new fractures grow around a magma sheet tip, either mechanically or thermo-mechanically, the properties (such as strength and elastic moduli) of the rock can change significantly (e.g. Kennedy et al., 2022; Singh et al., 2015; Wang & Konietzky, 2019; Lavallee and Kendrick, 2021). There are generally very few data on the thermoelastic properties of rock and how these properties evolve with temperature. However, tests on granitic rocks show a strongly non-linear thermal expansion co-efficient relation with temperature (Wang &

84 Konietzky, 2019). For example, the coefficient of thermal expansion becomes around
85 seven times higher and the elastic modulus decreases by approximately 30 GPa
86 when granite is heated from room temperature to 600 °C (Wang & Konietzky, 2019).
87 Therefore, if these conditions are not incorporated, simulations of crustal magma
88 transport and storage may become erroneous. Hence, a modelling approach to
89 consider the influence of temperature on altering stress state around magma sheets
90 over the common timescales of intrusion is required.
91

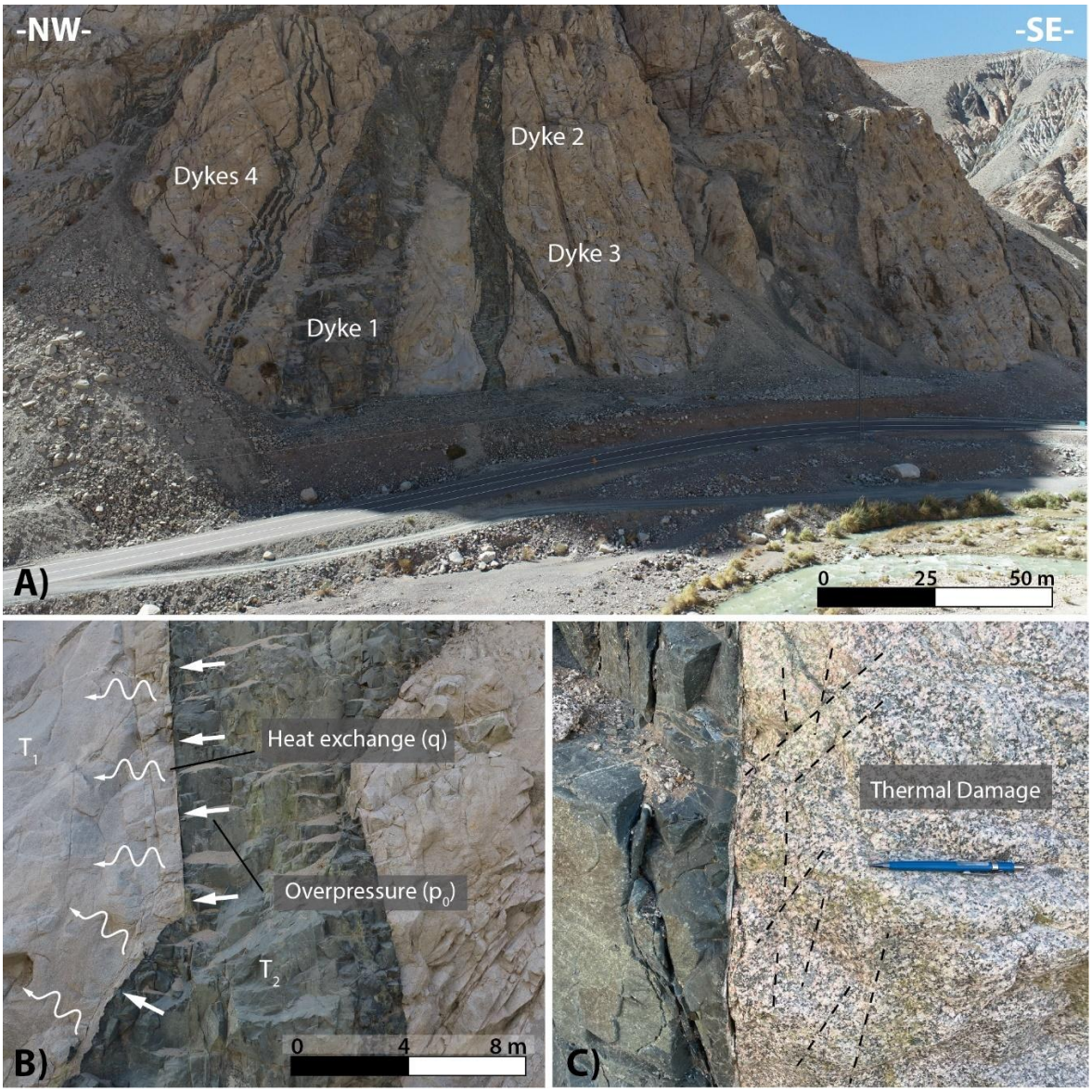


Figure 1. A) Photograph of an outcrop in Rio Turbio Valley, Coquimbo Region, Chile. Numerous dykes of different widths are exposed along the valley. B) In a wide dyke, magma has sufficient time to exchange heat and exert pressure on the host rock. C) Potential alteration and damage caused by the action of thermal stress in the surrounding host rock.

In this study, we modelled the local stresses around a dyke tip using three different constitutive models. As a reference, we used a pure elastic model in which thermal

effects were neglected. This type of model has been widely used in dyke propagation modelling (Gudmundsson, 2020). Then, we implement a coupled thermo-elastic model assuming rock property constants, and finally a non-linear coupled thermo-elastic model where rock properties become temperature-dependent. As the non-linearities of the five thermo-mechanical constants may lead to numerical instabilities, we performed a sensitivity analysis to choose the variables that most influence the local stress around a emplaced dyke. The aim was not to predict stresses associated with any particular dyke intrusion or geometry but instead to assess the potential for thermal loading related to inherent rock properties and timescales.

METHODOLOGY

Governing equations

We solved the coupled, transient thermoelastic problem (Duhamel–Neumann relations; Duhamel, 1837; Neumann & Meyer, 1885; Biot, 1956) on a two-dimensional vertical cross-section under plane-strain conditions. Latent heat and other energy sources related to phase changes were neglected. The temperature dependence of the material properties (Table 2) is taken from experiments on granite and includes the effect of the α–β quartz transition at 573 °C. In tension-positive form, the system is:

$$\rho c_v \frac{\partial \theta}{\partial t} - \nabla \cdot (k \nabla \theta) + k\,(\theta_0 + 273.15) tr\left(\frac{\partial \boldsymbol{\varepsilon}}{\partial t}\right) = 0 \quad (1)$$

$$\nabla \cdot \boldsymbol{\sigma} = 0 \quad (2)$$

$$\boldsymbol{\sigma} = \lambda tr(\boldsymbol{\varepsilon})\boldsymbol{I} + 2\mu\boldsymbol{\varepsilon} - \alpha(3\lambda + 2\mu)(\theta - \theta_0)\boldsymbol{I} \quad (3)$$

$$\varepsilon = \frac{1}{2}(\nabla u + \nabla u^T) \quad (4)$$

$$\lambda = \frac{\nu E}{(1+\nu)(1-2\nu)} \quad (5)$$

$$\mu = \frac{E}{2(1+\nu)} \quad (6)$$

121

122 where θ is temperature (°C), t is time, ρ is density, c_v is specific heat capacity, k is
123 thermal conductivity, σ and ε are the stress and strain tensors, u is displacement, I
124 is the identity tensor, and λ and μ are the Lamé parameters. $\theta_0(z)$ is the background
125 (pre-intrusion) geotherm, and the thermoelastic coefficient is κ = α(3λ + 2μ) = αE/(1
126 − 2v), with α the coefficient of thermal expansion. The coupling term in Eq. 1 uses
127 the absolute background temperature, θ_0 + 273.15 (in °C) its magnitude relative to
128 the heat-storage term is of order 10^{-3}.

129

130 Because rock mechanics uses compression positive, results are reported with the
131 sign reversed relative to Eqs. 1–6. σ_1 and σ_3 denote the maximum and minimum
132 principal stresses, with compression positive, so that $\sigma_3 < 0$ indicates net tension.

133

134 **Material properties**

135 Two thermo-mechanical models were considered. In the first model, the so-called
136 linear model, the thermal and mechanical parameters are considered constant and
137 their values are typically measured at room temperature (see Table 1). Then, a more
138 complex model was implemented, the so-called non-linear model, where the

parameters α, c_v, k, E, and ν are considered to be non-linear functions of temperature. Currently, there is a sparsity of thermo-mechanical data on crystalline rocks at elevated temperatures; therefore, our model is based on the experimentally derived curves described by Wang & Konietzky, (2019) as shown in Table 2.

Table 1. Thermal and mechanical parameters of the linear model measured at room temperature.

Thermo-mechanical Parameters			
Coefficient of thermal expansion	α	$8 \cdot 10^{-6}$	1/°C
Specific heat capacity	c_v	820	J/kg°C
Thermal conductivity	k	9360	J/hours/m°C
Elastic modulus	E	40	GPa
Poisson's ratio	ν	0.3	-

Table 2. Thermal and mechanical parameters as functions of temperature included in the non-linear model. Subscript 0 indicates the value of the parameter measured at room temperature (see Table 1). Data derived from Wang and Konietzky (2019).

Thermo-mechanical Parameters	
Coefficient of thermal expansion	$\alpha(\theta) = \begin{cases} \alpha_0(0.8383 - 0.00142\theta)^{(-1/1.7085)}, & \theta \leq 573°C \\ \alpha_0(-5.4160 + 0.0095\theta)^{(-1/1.5719)}, & 573°C < \theta \leq 625°C \\ 1.5131\alpha_0, & \theta > 625 \end{cases}$

Specific heat capacity	$c_v(\theta) = \begin{cases} c_{v0}(0.957 + 6.59 \cdot 10^{-4} \cdot \theta), & \theta \leq 575°C \\ c_{v0}(1.173 + 1.238 \cdot 10^{-4} \cdot \theta), & \theta > 575°C \end{cases}$
Thermal conductivity	$k(\theta) = k_0(-5.8126 + 6.8485 \cdot 0.9995^{\theta} + 0.002172\theta)$
Elastic modulus	$E(\theta) = \begin{cases} \dfrac{1.2665 \cdot E_0}{1 + e^{-1.43+0.0034 \cdot \theta}}, & \theta \leq 600°C \\ \dfrac{E_0}{-109.953 + 17.542 \cdot \ln \theta}, & \theta > 600°C \end{cases}$
Poisson's ratio	$\nu(\theta) = \begin{cases} \nu_0(1.0052 - 7 \cdot 10^{-4} \cdot \theta), & \theta \leq 600°C \\ \dfrac{2.24 \cdot \nu_0}{1 + e^{13.11-0.02 \cdot \theta}}, & \theta > 600°C \end{cases}$

Model domain and boundary conditions

The model domain consists of a 6 km wide and 3 km deep cross-section hosting a dyke of 500 m length and 10 m width, which was modelled as an elliptical, vertically oriented cavity with the top at a depth of 1250 m. Since the aim was to explore the influence of temperature effects under similar conditions, no other geometries were considered. The boundary conditions are divided into thermal and mechanical conditions. To solve the heat conduction equation, a depth-dependent temperature was set at the outer edges of the domain according to the expression $\theta = 15 + 30z$ (°C) (Browning et al., 2021). In addition, it was established that the magma in contact with the host rock had a constant temperature of 800 °C, simulating the instantaneous magma emplacement temperature. The magma is treated as an isothermal, non-convecting heat source and its cooling is not modelled. The 10 m wide intrusion cools on a timescale of thousands of hours, much longer than the 120 h simulated.Regarding the mechanical boundary conditions, a passive tectonic

environment was modelled, in which displacements are constrained at $u_x = 0$ at the lateral edges, and the lower edge displacement is constrained in both directions, the surface is free to move, and in the inner cavity a Neumann boundary condition is established, in which the magma exerts a modest overpressure p_0 of 0.2 MPa on the surrounding rock. Figure 2 graphically summarizes the geometry and boundary conditions of the model. The mesh size and time step are the key variables in solving the problem. As magma generates a high-temperature gradient on the rock contact at the initial condition, the Gibbs phenomenon (Gottlieb & Shu, 1997; Zhang, 2022) is observed, where an anomalous negative temperature appears on the nodes around the internal boundary. To avoid this issue, the node distance next to the dyke should be less than 1 m. A similar case occurs with stress, where anomalous jumps are controlled using mesh sizes below 0.1 m. The magma itself neither convects nor conducts (Rodriguez et al., 2015; Douglas et al., 2016) but simply imparts a temperature field on the surrounding rock. Since our aim is to determine the potential of temperature distribution, thermal stress and parameters, all of the models assume the same geometry and thermal and mechanical properties.

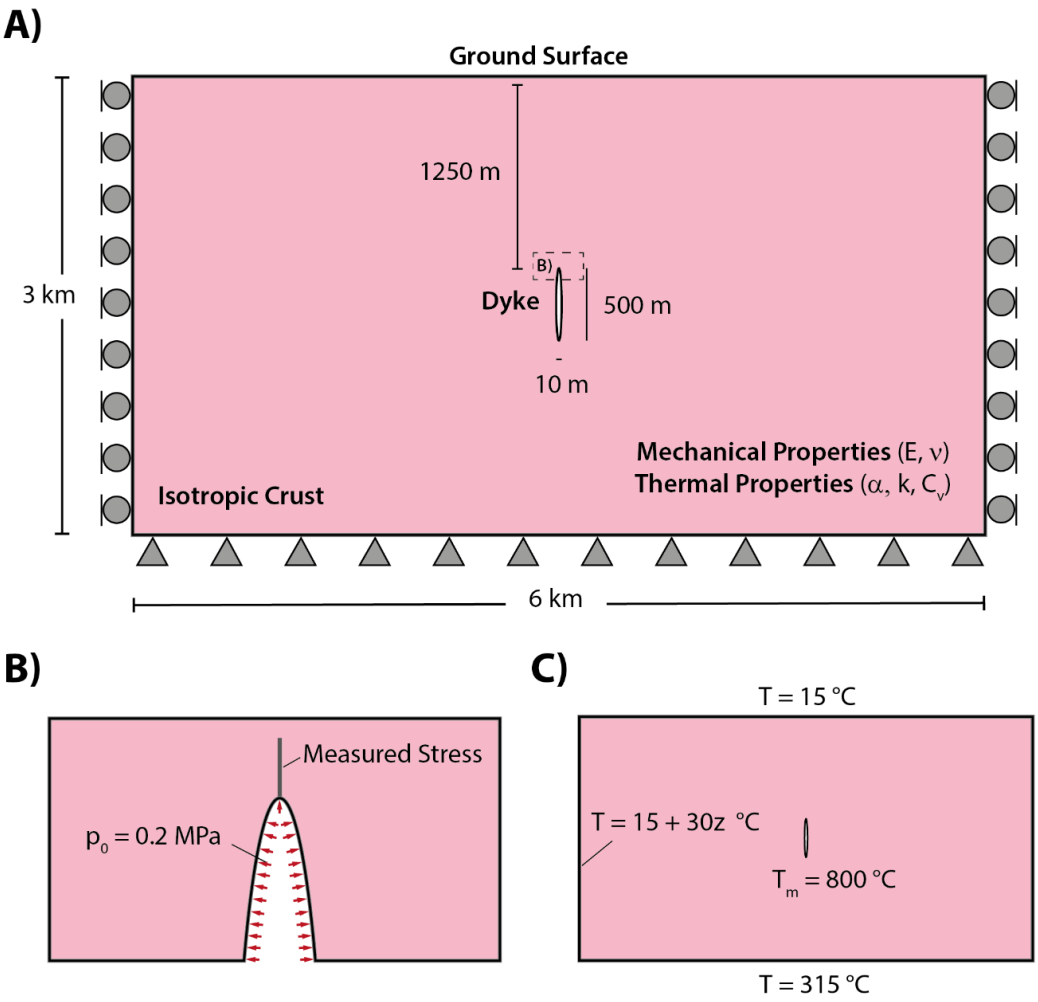


Figure 2. *Schematic representation of the numerical model to be developed. A) Geometry of the model and mechanical boundary conditions. B) Zoom to the model showing the mechanical boundary condition in the elliptical cavity, where (0.2 MPa) overpressure is applied. C) Thermal boundary conditions, where a pre-described temperature was set at the outer and inner edges.*

RESULTS

Figure 3 depicts the first results of the most complex non-linear thermo-mechanical model after 24 hours of dyke intrusion. At this point, a roughly 2-meter wide

symmetrical thermal halo was formed around the modelled dyke within the surrounding host rock (Figure 3). As the temperature within the host rock increased over this time, thermal expansion promoted elevated thermal stress (Figure 3D and E). Within 2 meters from the tip of the dyke, the consequence of this thermal deformation was that the local stress changed from a dominantly regime ($\sigma_3 < 0$) (Figure 4) to a dominantly compressive regime. The resulting thermal stress generated very high σ_3 and σ_1 of 180 and 700 MPa, respectively, for the tested conditions. These are very high stresses, but they relate to grain scale thermal deformation and thermal stress (Meredith et al., 2001) and are hence reasonable. Only tensile stress is found within <10 cm at the tip of the dyke in the purely elastic model, this is consistent with prior findings (Gudmundsson, 2011). However, in both the linear and non-linear thermo-mechanical models, over the same area, there are large compressive stresses (Figure 4). The main difference between the linear and non-linear models is the way in which the compressive stresses vary with temperature (distance from the dyke tip). The stress essentially follows the distribution of temperature in the linear model, such that as temperature decreases from 800 degrees to the background temperature field within around 1 m of the dyke tip, the stress decreases from around 700 MPa to around 90 MPa. Conversely, in the non-linear model with the same temperature distribution, the stress increases from around 200 MPa to around 600 MPa within the first 10 cm peaking at around 525 degrees and then decreases to 100 MPa.

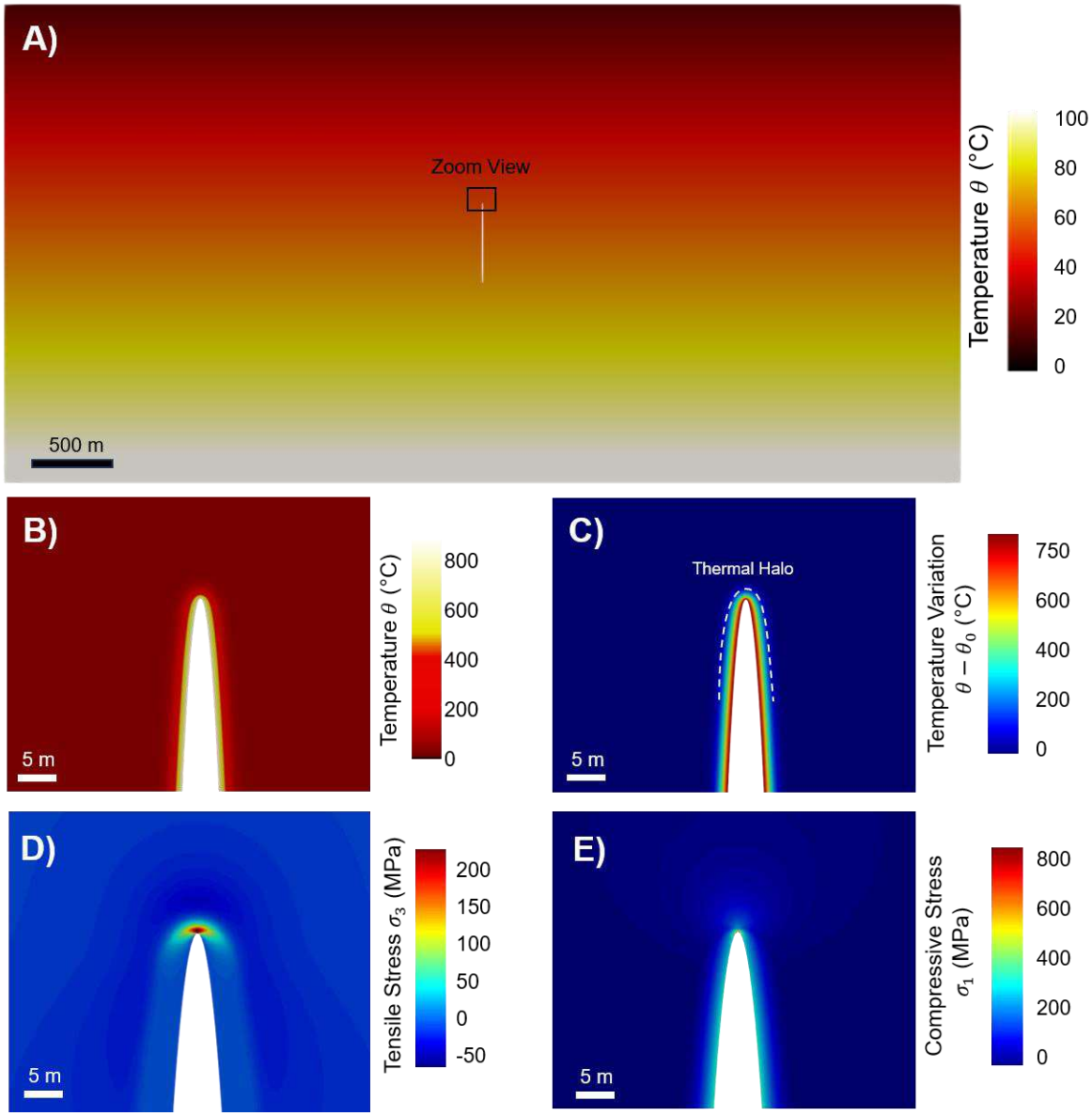
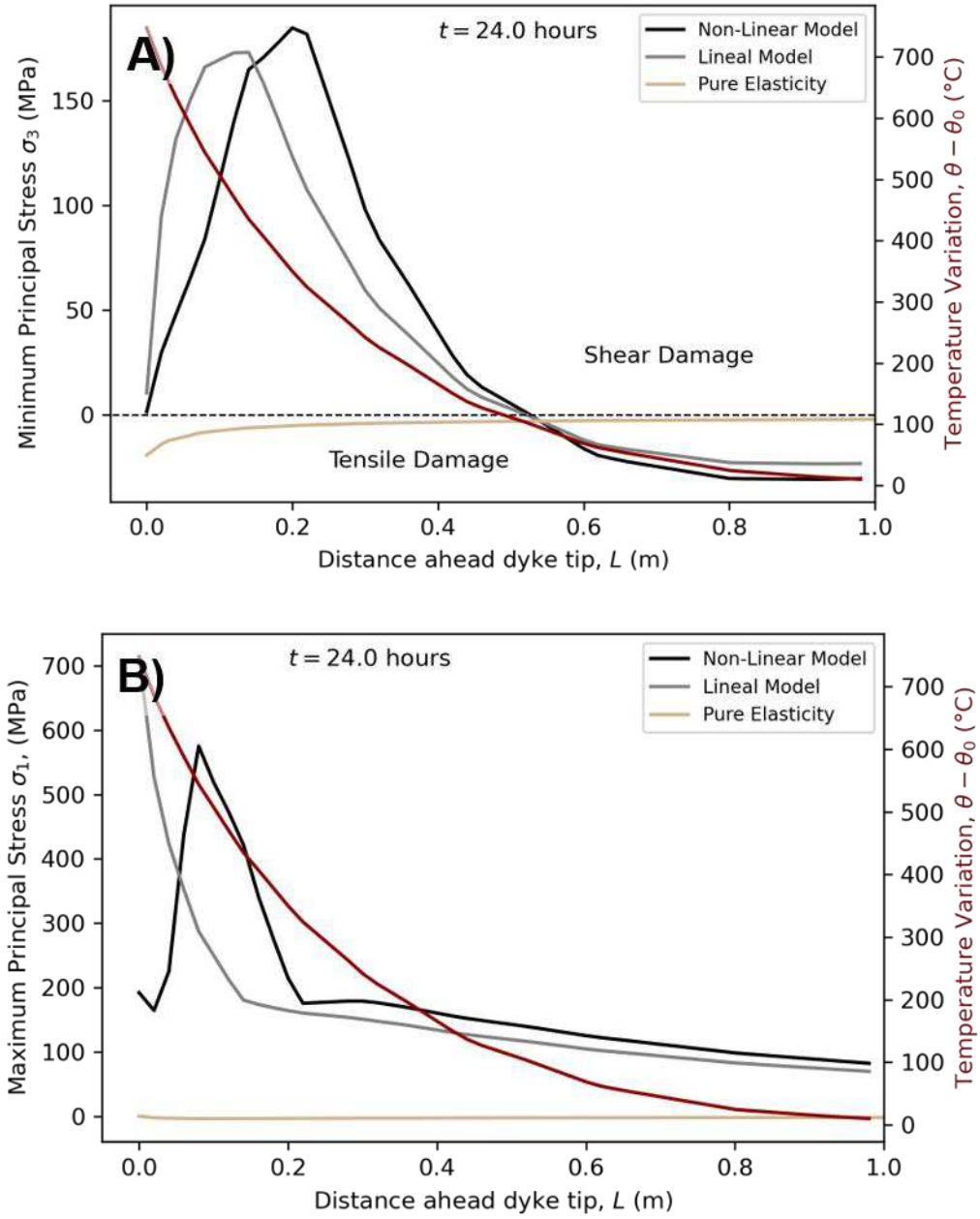


Figure 3. Results from a representative non-linear thermo-mechanical model. A) Large-scale vertical thermal profile of the crust surrounding a dyke, with the zoomed-in region indicated in black. B) Close-up view of the temperature distribution around the dyke tip within the zoomed-in region 24 hours after intrusion. C) Thermal halo surrounding the dyke tip. D) Stress distribution (σ_3) around the dyke tip. E) Stress distribution (σ_1) around the dyke tip.



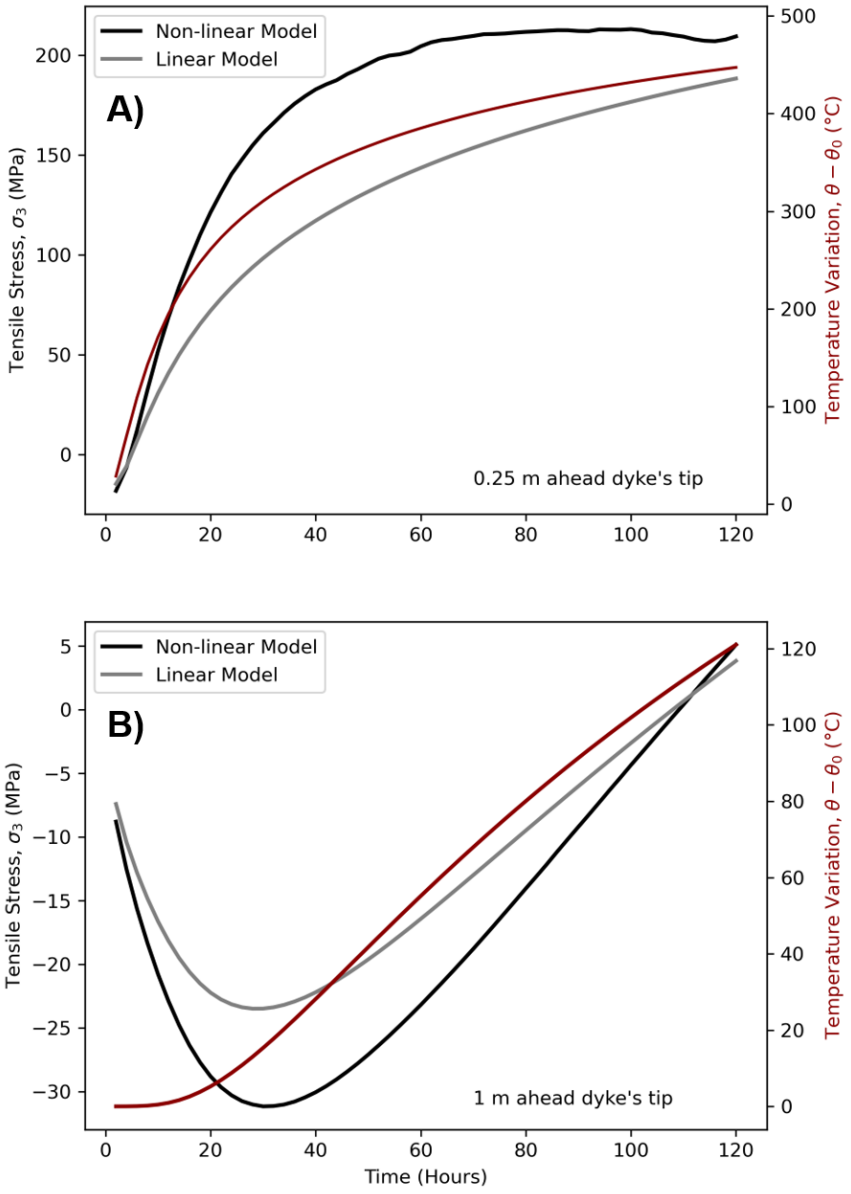
225

226 *Figure 4. Comparison of stress distribution (σ_1 and σ_1) and temperature variation ($\theta - \theta_0$)*
227 *after 24 hours of simulation for three models: Non-Linear, Linear, and Pure Elasticity (note*
228 *for the elasticity models: there is no temporal element – the data is from the initial point of*
229 *the simulation).*

230

231

σ_3 in the process zone is predominantly compressive, as is illustrated in Figure 5A where the temporal evolution of σ_3 and temperature variation at a point 0.25 meters ahead the dyke's tip over a period of 120 hours is shown. $\sigma_3$in the non-linear thermo-mechanical model increases rapidly during the initial phase, reaching a peak of approximately 200 MPa before decreasing and stabilizing at approximately 190 MPa. The linear model also showed an increase in σ_3, but at a slower rate, peaking at approximately 150 MPa. In contrast, far ahead of the dyke tip (Figure 5B), σ_3 for the non-linear model decreases initially, reaching a minimum of approximately -30 MPa around 30 hours after magma intrusion, before increasing to around 5 MPa by the end of the period. The linear model also showed an initial decrease in σ_3, reaching a minimum of about -23 MPa around 30 hours, before increasing and stabilizing around 3 MPa by the end of the period. Comparing both thermo-mechanical models, the non-linear model predicts a greater range of σ_3 compared to the linear model, indicating the significant impact reflecting the non-linearity of thermal expansion and other rock properties with temperature.



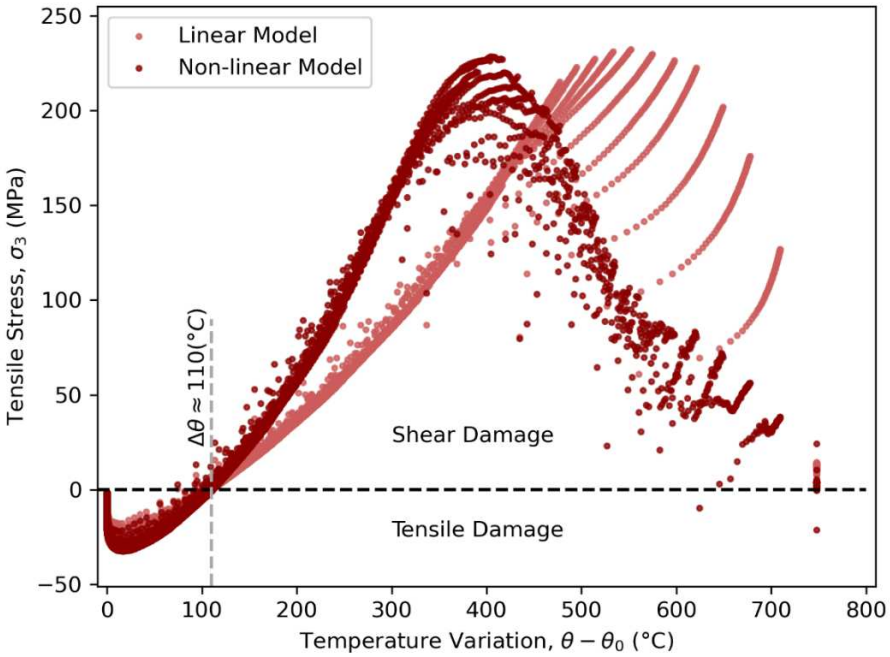
248

249 *Figure 5. Comparison of tensile stress (σ_3) and temperature variation ($\theta - \theta_0$) over time for*
250 *linear and non-linear models at two different distances ahead of a dyke's tip. A) Process*
251 *zone (at 0.25 m from the dyke tip) and B) Distal zone (at 1 m from the dyke tip).*

252

253 The relationship between $\sigma_3$and temperature variation for both the linear and non-
254 linear models is depicted in Figure 5. Thermo-mechanical models indicate a rise in

$\sigma_3$as the temperature increases, reaching a peak of approximately 200 MPa. However, there is a critical temperature variation of around 110°C, which can be linked to a transition from tensile to compressive stress and may therefore further be responsible for a change in the dominant form of crack damage, changing from dilatant to shear. Moreover, the non-linear model reaches its maximum $\sigma_3$when the temperature of the rock has been elevated by 400°C, whereas the linear model attains this when the temperature has risen to almost 600°C. The results obtained for the compressive stress (σ_1) also exhibited an increase with rising temperatures. However, the curves in both the linear and non-linear models revealed distinct differences in how compressive stress responds to temperature variation. In the linear model, the stress displayed a smoother and more gradual increase, while the non-linear model showed a more pronounced peak around 510°C before decreasing at the same rate before the maximum value.

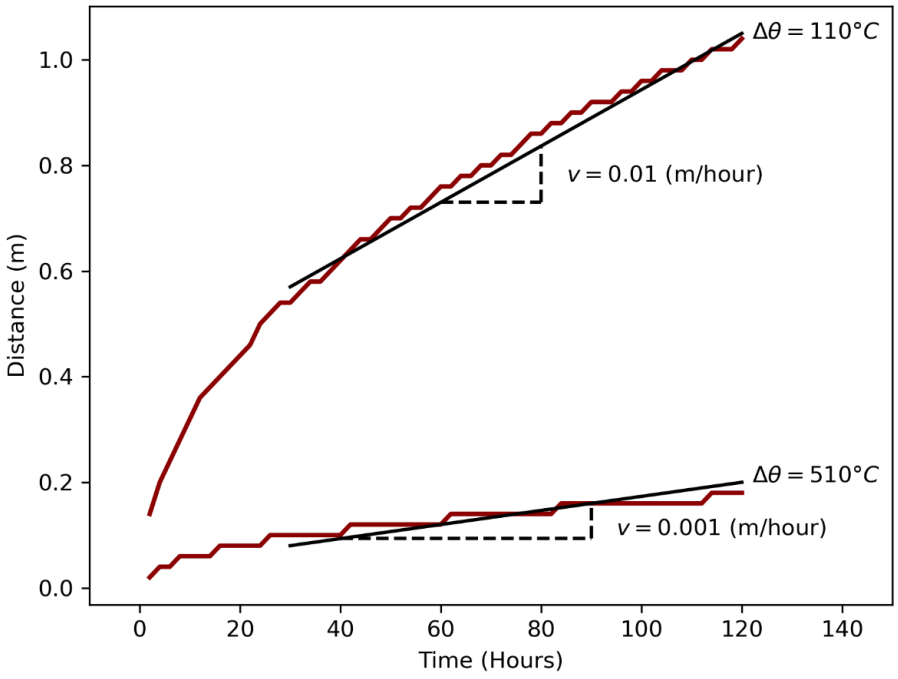


268

269 *Figure 6. Relationship between tensile stress (σ_3) and temperature variation ($\theta - \theta_0$) for*
270 *both linear and non-linear thermo-mechanical models. Each point represents a transient*
271 *FEM solution at a particular time step and location.*

272 The rate at which heat is transferred through the modelled rock is shown in Figure
273 7, which depicts the progression in time of two isotherms around a dyke. The upper
274 curve in Figure 7 illustrates propagation of the isotherm at 110°C, which is
275 responsible for the shift from tensile to compressive stress. This isotherm moves at
276 a rate of 0.01 meters per hour, and after 120 hours, it has progressed approximately
277 1 meter from the magma intrusion. The isotherm of 510°C, which is the temperature
278 at which compressive stress reaches a maximum in most models (Figure 6),
279 propagates at a slower rate of 0.001 m/hour reaching around 0.2 meters after only
280 120 hours (< 6 days).

281



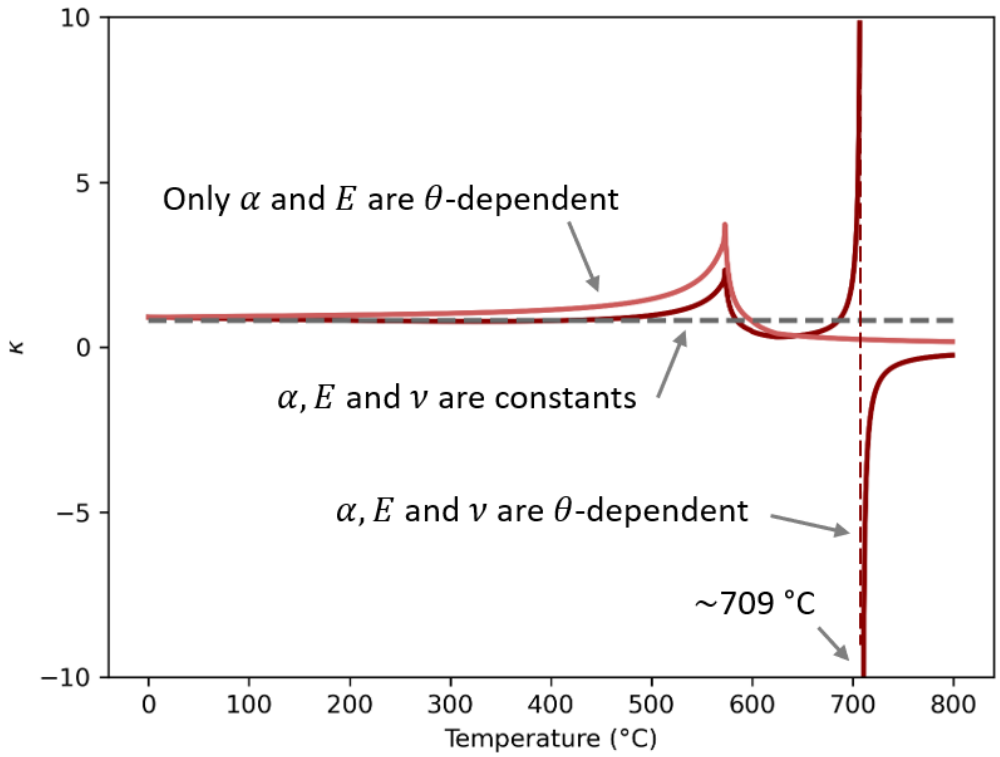
282

283 *Figure 7. Propagation rate of isotherms around the modelled dyke after magma intrusion for*
284 *two temperatures, 110℃ and 510℃.*

285 The thermal component of the stress shown in equation 7 is controlled by the term
286 $\kappa = \alpha(3\lambda + 2\mu)$. If the three parameters involved in the equation 7 (E, ν, and α) are
287 temperature-dependent, the term κ becomes undefined at approximately 709°C, as
288 depicted in Figure 8, resulting in the non-convergence of models in which the magma
289 temperature exceeds that threshold. To avoid this problem and model cases with
290 higher magma temperatures, we kept the Poisson's ratio constant.

$$\boldsymbol{\sigma} = \lambda tr(\boldsymbol{\varepsilon})\boldsymbol{I} + 2\mu\boldsymbol{\varepsilon} - \underbrace{\alpha(3\lambda + 2\mu)}_{\kappa}(\theta - \theta_0)\boldsymbol{I} \quad (7)$$

291



292

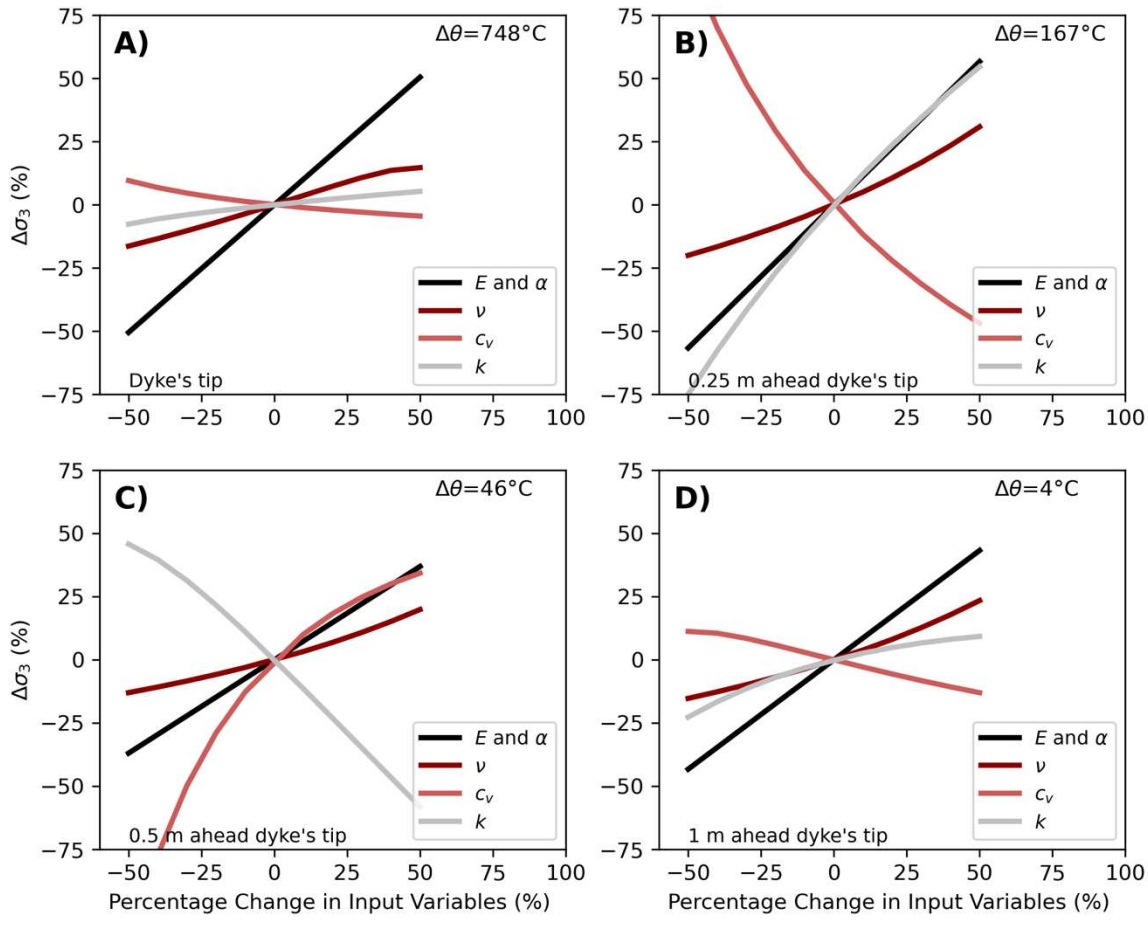
293 *Figure 8. Thermoelastic coefficient (k) as a function of temperature for different conditional*
294 *dependencies between thermal expansion co-efficient (α), Young's moduli (E), Poisson ratio*
295 *(ν) and temperature change (θ).*

296

297 Additionally, a sensitivity analysis was carried out to determine perturbations in each
298 input variable (Elastic modulus, Poisson's ratio, coefficient of thermal expansion,
299 specific heat and thermal conductivity of the rock). To do this, we modified each
300 parameter by as much as 50% from the reference model and calculated the
301 respective variation in the amount of σ_3, at four distances from the dyke; at the tip,
302 and at 0.25, 0.5 and 1 meters ahead the dyke (Figure 9). In each model, modification
303 of the elastic modulus and coefficient of thermal expansion generate the same effect.
304 Both at the tip of the dyke and at 1 meter ahead of the dyke tip, both the elastic
305 modulus and the coefficient of thermal expansion produce the largest impact on the

306 σ_3, an increase of 50% in these parameters also produces an increase of more than
307 50% in the amount of tensile stress. The second most important parameters are
308 Poisson's ration and specific heat capacity. These both generate differences of
309 between around 10-15% in tensile stress at <1m from the dyke tip. However, whilst
310 Poisson's ratio exhibits a positive correlation, indicating increases in Poisson's ratio
311 generate larger amounts of tensile stress, the specific heat capacity displays an
312 inverse correlation. This implies that an increase in specific heat capacity may act to
313 reduce the total amount of tensile stress.

314



315

Figure 9. Sensitivity analysis of the change in the amount of tensile stress ($\Delta\sigma_3$) as a function of the change of different input variables. A) Relations calculated directly at the dyke tip, at a temperature change of 748 °C. B) 0.25 m ahead of the dyke tip, at a temperature change of 167 °C. C) 0.5 m ahead of the dyke tip at a temperature change of 46 °C. D) 1 m ahead of the dyke tip, at a temperature change of only 4 °C.

DISCUSSION

We introduce comparison of temperature distributions and resulting thermal stress surrounding a 10 m wide and 500 m long dyke using both linearly dependent and non-linear thermo-mechanical models resolved through Finite Elements. The models simulate thermal stress within the uppermost portion of the Earth's crust. The model is a first step that should logically be expanded to consider other magma geometries, sizes and depths, such as sills and inclined sheets. We do attempt to impose failure criterion and so no fracture damage is generated, only the stress magnitudes and types that may be responsible for the generation of new damage. Further limitations of our model is that it does not consider an ambient stress field, is two-dimensional, considers a homogeneous crustal segment and does not consider time-dependent or fluid derived processes. Whilst acknowledging the various model limitations we do now attempt to utilize the general FEM model findings to consider a conceptual model divided into three stages relating to the interpreted fracture mechanics governing the process zone around the tip of the dyke

(Figure 10). The model is placed in the context of well-observed dyke injection events to consider the interplay of magma emplacement and thermal perturbation.

During the first stage (Stage I), dyke propagation is primarily driven by tensile stress arising from magma overpressure. During this period, thermo-mechanical stresses play a negligible role in controlling the upward or lateral movement of magma since there is insufficient time to heat the surrounding rock to a level that produces thermal stress and thermal damage (Browning et al., 2016). Seismicity during the 2014-2015 Bárðarbunga-Holuhraun rifting event in Iceland revealed the episodic propagation of dykes, with velocities ranging between 0.08 m/s and 1.3 m/s (Agustsdottir et al., 2016). In an earlier rifting episode in Krafla (Wright et al., 2012), propagation velocities ranged from 0.14 to 0.83 m/s. Additionally, during the Dabbahu rifting event between 2005 and 2010 in the Afar region, similar velocities were recorded (Wright et al., 2006), indicating a common feature in dyke propagation during rifting events (Davis and Biggs., 2026). Moreover, it reflects variations in the dynamics of the dyke, with sections that propagated more rapidly and others that moved more slowly or even temporarily arrested. Our models indicate that thermal perturbations and consequently stress; propagates into the host rock at velocities ranging from 0.001 to 0.01 m/h because most rock is a relatively poor conducting material. The thermal conductivity of rocks typically ranges from 0.40 to 7.00 $Wm\text{-}1K^{-1}$ (Čermák & Rybach, 1982). Low values are commonly observed in unconsolidated, dry sedimentary rocks, such as gravels and sands. Rocks with high quartz content, such as quartzite and sandstone, as well as water-saturated rocks, are the most effective heat conductors (Schön, 2015). However, their values are 1 or 2 order of magnitudes

lower that metals and other common materials used in engineering (Uher, 2004). Hence, the dyke's tip progresses faster than the heat is conducted in the surrounding host rock avoiding the production of significant temperature gradients (Gudmundsson, 2026) and thermal stresses. Thus, under these conditions a dyke behaves essentially as a hydraulic fracture driven mainly by the overpressure of the magma (generating dominantly Mode I fracture). This stage changes when the dyke becomes stalled or arrested, due to either decreasing magma flux (Gudmundsson, 2020) or by crustal heterogeneities generating stress barriers (Clunes et al., 2021; Drymoni et al., 2020).

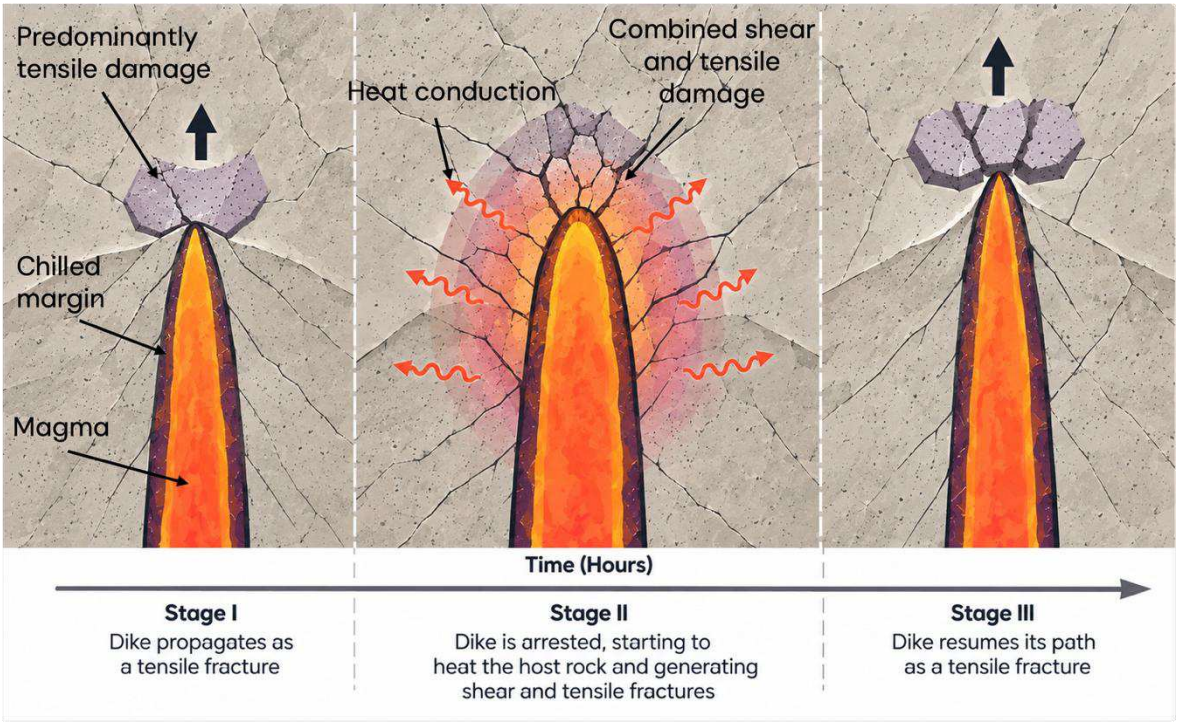


Figure 10. Conceptual temporal model of crustal dyke propagation and arrest in the crust considering pure elasticity (Stage I) as the dyke propagates faster than heat conduction into the surrounding host rock damages the rock, combined thermoelasticity (Stage II) related to temporary dyke stalling where thermal cracking and damage processes act to condition the surrounding rock, and then again pure elasticity as the dyke propagates dynamically (stage

III). Illustration modified using generative AI GPT-6 from an original hand drawn sketch and subsequently annotated.

Stage II initiates after magma emplacement. When a dyke becomes arrested for a significant period of time, the temperature difference between the magma and the host rock permits heat conduction through Fourier's law (Hahn and Ozisik, 2012). As temperature increases, volumetric expansion generates thermal stress in a centimetric halo around the dyke. This may lead to thermal damage during the heating and expansion phase (Daoud et al., 2020). Thermal damage acts to progressively alter the mechanical properties of the rock (Wang & Konietzky, 2019) directly impacting the newly induced stresses. In Stage II, compressive thermal stress overcomes purely elastic tensile stresses generated by the dyke overpressure (Browning et al., 2021), potentially modifying the local stress field such that future fracture growth may occur under mixed-mode loading conditions rather than under predominantly Mode I conditions. However, explicit simulation of fracture propagation would be required to confirm such a transition. While the thermo-mechanical models predict substantial changes in the stress field surrounding the dyke tip, they do not include fracture propagation or damage evolution. Consequently, the inferred transition from predominantly Mode I loading to mixed-mode conditions should be regarded as a mechanical interpretation of the stress state rather than a direct prediction of fracture behaviour. Further understanding of the dominant fracture modes has implications for the amount and style of related seismicity during dyke propagation (Woods et al., 2018). Further, the generation thermal damage may generate permeable pathways permitting fluid flow within and

around dykes. Together these processes may combine to permit an arrested dyke to resume its path once the thermal stresses have contributed to overcoming the local rock strength. Stage III is again characterized by a return to overpressure controlled (dominantly mode I) fracture when a dyke may resume its propagation path at a relatively rapid velocity.

CONCLUSIONS

1. We introduce a comparison of thermo-mechanical models that calculate the stress distribution ahead of an emplaced dyke in a transient state utilizing linear and non-linear thermal properties. These consider the influence of temperature on rock physical properties immediately adjacent to a newly emplaced intrusion and the potential consequence in terms of thermal fracture damage, although damage is not modelled per se.
2. When the influence of thermal induced stress is modelled, increments of fracture growth may become increasingly influenced by both tensile and compressive stresses, creating conditions consistent with mixed-mode fracture damage. The present models do not explicitly simulate fracture propagation, but they indicate that thermal stresses could modify the mechanical environment surrounding an arrested dyke.
3. A conceptual model of magma propagation is presented, where thermal stress becomes important in preparing host rock for continued propagation during periods of extended magma arrest.

4. In our thermo-mechanical model, the most sensitive model inputs are the elastic moduli (E) and the coefficient of thermal expansion (α) directly at the dyke tip. The importance of the other model parameters vary considerably depending on the position and the temperature reached by the rock.

ACKNOWLEDGEMENTS

This research was supported by La Agencia Nacional de Investigación y Desarrollo (ANID) through Chilean National Fund for Scientific and Technological Development (FONDECYT) projects Fondecyt 1240188 - OFFSET. Jorge Cortez acknowledged support from ANID 21210339. The authors would like to express their gratitude to SynergyGrid, the server infrastructure provided by the Faculty of Engineering of the University of La Serena.

A note on Jorge Cortez, who sadly passed away on the 29th May 2026 aged 33. Jorge will be remembered as an excellent colleague, a loving person and a dear friend. I leave this note in a paper that is the fruit of his work and of his love for science. He is, and will be, deeply missed.



REFERENCES

Barnett, Z. A., & Gudmundsson, A. (2014). Numerical modelling of dykes deflected into sills to form a magma chamber. *Journal of Volcanology and Geothermal Research*, *281*, 1–11.

Bartlett, R. W. (1969). Magma convection, temperature distribution, and differentiation. *American Journal of Science*, *267*(9), 1067–1082.

Biot, M. A. (1956). Thermoelasticity and irreversible thermodynamics. *Journal of Applied Physics*, *27*(3), 240–253.

Brady, B. H. G., & Brown, E. T. (2006). *Rock mechanics: for underground mining*. Springer science & business media

Browning, J., Drymoni, K. and Gudmundsson, A., 2015. Forecasting magma-chamber rupture at Santorini volcano, Greece. *Scientific reports*, *5*(1), p.15785

Browning, J., Meredith, P. and Gudmundsson, A., 2016. Cooling-dominated cracking in thermally stressed volcanic rocks. *Geophysical Research Letters*, *43*(16), pp.8417-8425

Browning, J., Karaoğlu, Ö., Bayer, Ö., Turgay, M. B., & Acocella, V. (2021). Stress fields around magma chambers influenced by elastic thermo-mechanical deformation: implications for forecasting chamber failure. *Bulletin of Volcanology*, *83*, 1–13

Burchardt, S., Bazargan, M., Gestsson, E.B., Hieronymus, C., Ronchin, E., Tuffen, H., Heap, M., Davidson, J., Kennedy, B., Hobé, A. and Saubin, E., 2022. Geothermal potential of small sub-volcanic intrusions in a typical Icelandic caldera setting. *Volcanica*, *5*(2), pp.477-507.

Čermák, V., & Rybach, L. (1982). Thermal conductivity and specific heat of minerals and rocks. *Landolt-Börnstein: Numerical Data and Functional Relationships in Science and Technology, New Series, Group V (Geophysics and Space Research), Volume Ia,(Physical Properties of Rocks), Edited by G. Angenheister, Springer, Berlin-Heidelberg*, 305–343.

Corti, N., Bonali, F.L., Russo, E., Drymoni, K., Mariotto, F.P., Gudmundsson, A., Esposito, R., Cavallo, A. and Tibaldi, A., 2023. Feeders vs arrested dikes: a case study from the Younger Stampar eruption in Iceland. *Journal of Volcanology and Geothermal Research*, *443*, p.107914.

Clunes, M., Browning, J., Cembrano, J., Marquardt, C., & Gudmundsson, A. (2021). Crustal folds alter local stress fields as demonstrated by magma sheet—Fold interactions in the Central Andes. *Earth and Planetary Science Letters*, *570*, 117080.

Daoud, A., Browning, J., Meredith, P. G., & Mitchell, T. M. (2020). Microstructural controls on thermal crack damage and the presence of a temperature-memory effect during

cyclic thermal stressing of rocks. *Geophysical Research Letters*, *47*(19), e2020GL088693.

Davis, T., & Biggs, J. (2026). Constraints on magma source conditions from hydraulic fracture models and seismic observations of dyke tip deceleration. Eartharxiv.

Delaney, P. T., Pollard, D. D., Ziony, J. I., & McKee, E. H. (1986). Field relations between dikes and joints: Emplacement processes and paleostress analysis. *Journal of Geophysical Research: Solid Earth*, *91*(B5), 4920-4938.

Douglas, M.M., Geyer, A., Álvarez-Valero, A.M. and Martí, J., 2016. Modeling magmatic accumulations in the upper crust: Metamorphic implications for the country rock. *Journal of Volcanology and Geothermal Research*, *319*, pp.78-92.

Drymoni, K., Browning, J., & Gudmundsson, A. (2020). Dyke-arrest scenarios in extensional regimes: Insights from field observations and numerical models, Santorini, Greece. *Journal of Volcanology and Geothermal Research*, *396*, 106854.

Drymoni, K., Browning, J., & Gudmundsson, A. (2021). Volcanotectonic interactions between inclined sheets, dykes, and faults at the Santorini Volcano, Greece. *Journal of Volcanology and Geothermal Research*, *416*, 107294.

Duhamel, J. M. C. (1837). Second memoire sur les phenomenes thermo-mecaniques. *Journal de l'École Polytechnique*, *15*(25), 1–57.

Ersoy, H., Kolaylı, H., Karahan, M., Harputlu Karahan, H. and Sünnetci, M.O., 2019. Effect of thermal damage on mineralogical and strength properties of basic volcanic rocks exposed to high temperatures. Bulletin of Engineering Geology and the Environment, 78, pp.1515-1525.

Fialko, Y. A., & Rubin, A. M. (1999). Thermal and mechanical aspects of magma emplacement in giant dike swarms. *Journal of Geophysical Research: Solid Earth*, *104*(B10), 23033-23049.

Gottlieb, D., & Shu, C.-W. (1997). On the Gibbs phenomenon and its resolution. *SIAM Review*, *39*(4), 644–668.

Green, D. H., Falloon, T. J., Eggins, S. M., & Yaxley, G. M. (2001). Primary magmas and mantle temperatures. *European Journal of Mineralogy*, *13*(3), 437–452.

Gregg, P. M., De Silva, S. L., & Grosfils, E. B. (2013). Thermomechanics of shallow magma chamber pressurization: Implications for the assessment of ground deformation data at active volcanoes. *Earth and Planetary Science Letters*, *384*, 100–108.

Gudmundsson, A. (2006). How local stresses control magma-chamber ruptures, dyke injections, and eruptions in composite volcanoes. *Earth-science reviews*, *79*(1-2), 1-31.

Gudmundsson, A. (2011a). Deflection of dykes into sills at discontinuities and magma-chamber formation. *Tectonophysics*, *500*(1–4), 50–64.

Gudmundsson, A. (2011b). *Rock fractures in geological processes*. Cambridge University Press.

Gudmundsson, A., Lecoeur, N., Mohajeri, N. and Thordarson, T., 2014. Dike emplacement at Bardarbunga, Iceland, induces unusual stress changes, caldera deformation, and earthquakes. *Bulletin of Volcanology*, *76*, pp.1-7.

Gudmundsson, A. (2020). *Volcanotectonics: Understanding the structure, deformation and dynamics of volcanoes*. Cambridge University Press.

Gudmundsson, A. (2026). The effects of stress gradients on faulting and dyke emplacement, with applications to Santorini and Iceland. *Geological Society, London, Special Publications*, *560*(1), 173-215

Hahn, D. W., & Özisik, M. N. (2012). *Heat conduction*. John Wiley & Sons.

Head, M., Hickey, J., Thompson, J., Gottsmann, J. and Fournier, N., 2022. Rheological controls on magma reservoir failure in a thermo-viscoelastic crust. Journal of Geophysical Research: Solid Earth, 127(7), p.e2021JB023439.

Healy, D., Rizzo, R. E., Duffy, M., Farrell, N. J., Hole, M. J., & Muirhead, D. (2018). Field evidence for the lateral emplacement of igneous dykes: Implications for 3D mechanical models and the plumbing beneath fissure eruptions. *Volcanica*, *1*, 85-103.

Hickey, J., Gottsmann, J., Nakamichi, H., & Iguchi, M. (2016). Thermomechanical controls on magma supply and volcanic deformation: application to Aira caldera, Japan. *Scientific Reports*, *6*(1), 32691.

Hofer-Apostolidis, K., Cembrano, J., Browning, J., Pérez-Flores, P., Mitchell, T.M., Meredith, P.G., Rojas, F. and Xu, T., 2024. Fracture growth and damage zone evolution in fault-vein systems determined through scaling relations in alteration halo-bearing hydrothermal veins. *Journal of Structural Geology*, p.105219.

Karaoğlu, Ö., Bayer, Ö., Turgay, M. B., & Browning, J. (2020). Thermomechanical interactions between crustal magma chambers in complex tectonic environments: Insights from Eastern Turkey. *Tectonophysics*, *793*, 228607.

Kennedy, B., Heap, M., Burchardt, S., Villeneuve, M., Tuffen, H., Gilg, H. A., Davidson, J., Duncan, N., Saubin, E., & Gestsson, E. B. (2022). Thermal impact of dykes on ignimbrite and implications for fluid flow compartmentalisation in calderas. *Volcanica*, *5*(1), 75–93.

Lavecchia, A., Clark, S.R., Beekman, F., Cloetingh, S.A. and Burov, E., 2016. Thermal perturbation, mineral assemblages, and rheology variations induced by dyke emplacement in the crust. Tectonics, 35(5), pp.1137-1152.

Lavallée, Y. and Kendrick, J.E., 2021. A review of the physical and mechanical properties of volcanic rocks and magmas in the brittle and ductile regimes. *Forecasting and planning for volcanic hazards, risks, and disasters*, pp.153-238.

Loncar, M. and Huppert, H.E., 2022. Dyke cooling upon intrusion: Subsequent shape change, cooling regimes and the effect of further magma input. *Earth and Planetary Science Letters*, *593*, p.117687.

559 Liu, L., Ji, H., Elsworth, D., Zhi, S., Lv, X. and Wang, T., 2020. Dual-damage constitutive
560 model to define thermal damage in rock. International Journal of Rock Mechanics and
561 Mining Sciences, 126, p.104185.

562 Meredith, P.G., Knight, K.S., Boon, S.A. and Wood, I.G., 2001. The microscopic origin of
563 thermal cracking in rocks: An investigation by simultaneous time-of-flight neutron
564 diffraction and acoustic emission monitoring. *Geophysical research letters*, *28*(10),
565 pp.2105-2108.

566 Neumann, F. L., & Meyer, O. E. (1885). *Vorlesungen über die theorie der elasticität der*
567 *festen körper und des lichtäthers*. Druck und Verlag von BG Teubner.

568 Patel, R., Browning, J., Sarma, D.S. and Panda, A., 2022. Mechanical fragmentation and
569 thermal erosion of dyke adjacent host rocks induced by fluid-dynamic shear stress
570 and latent heat release in response to turbulent magma flow. Journal of Volcanology
571 and Geothermal Research, 429, p.107599.

572 Petford, N., Kerr, R. C., & Lister, J. R. (1993). Dike transport of granitoid magmas.
573 *Geology*, *21*(9), 845–848.

574 Poppe, S., Holohan, E.P., Galland, O., Buls, N., Van Gompel, G., Keelson, B., Tournigand,
575 P.Y., Brancart, J., Hollis, D., Nila, A. and Kervyn, M., 2019. An inside perspective on
576 magma intrusion: Quantifying 3D displacement and strain in laboratory experiments
577 by dynamic X-ray computed tomography. Frontiers in Earth Science, 7, p.62.

578 Pollard, D.D., 1973. Derivation and evaluation of a mechanical model for sheet intrusions.
579 Tectonophysics, 19(3), pp.233-269.

580 Rivalta, E., Taisne, B., Bunger, A.P. and Katz, R.F., 2015. A review of mechanical models
581 of dike propagation: Schools of thought, results and future directions. Tectonophysics,
582 638, pp.1-42.

583 Rodríguez, C., Geyer, A., Castro, A. and Villaseñor, A., 2015. Natural equivalents of
584 thermal gradient experiments. *Journal of Volcanology and Geothermal*
585 *Research*, *298*, pp.47-58.

586 Rubin, A. M. (1995). Propagation of magma-filled cracks. *Annual Review of Earth and*
587 *Planetary Sciences*, *23*(1), 287–336.

588 Ruz, J., Browning, J., Cembrano, J., Iturrieta, P., Gerbault, M., & Sielfeld, G. (2020). Field
589 observations and numerical models of a Pleistocene-Holocene feeder dyke swarm
590 associated with a fissure complex to the east of the Tatara-San Pedro-Pellado
591 complex, Southern Volcanic Zone, Chile. *Journal of Volcanology and Geothermal*
592 *Research*, *404*, 107033.

593 Schön, J. H. (2015). *Physical properties of rocks: fundamentals and principles of*
594 *petrophysics*. Elsevier.

595 Schmeling, H. and Zulauf, G., 2024. The physics of dyke and sill emplacement:
596 Solidification, visco-elasticity, stress evolution, and melt migration. Tectonophysics,
597 p.230367.

598 Sigmundsson, F., Hooper, A., Hreinsdóttir, S., Vogfjörd, K.S., Ófeigsson, B.G., Heimisson,
599 E.R., Dumont, S., Parks, M., Spaans, K., Gudmundsson, G.B. and Drouin, V., 2015.
600 Segmented lateral dyke growth in a rifting event at Bárðarbunga volcanic system,
601 Iceland. *Nature*, *517*(7533), pp.191-195.

602 Sigmundsson, F., Parks, M., Hooper, A., Geirsson, H., Vogfjörd, K.S., Drouin, V.,
603 Ófeigsson, B.G., Hreinsdóttir, S., Hjaltadóttir, S., Jónsdóttir, K. and Einarsson, P.,
604 2022. Deformation and seismicity decline before the 2021 Fagradalsfjall
605 eruption. *Nature*, *609*(7927), pp.523-528.

606 Singh, B., Ranjith, P.G., Chandrasekharam, D., Viete, D., Singh, H.K., Lashin, A. and Al
607 Arifi, N., 2015. Thermo-mechanical properties of Bundelkhand granite near Jhansi,
608 India. *Geomechanics and Geophysics for Geo-Energy and Geo-Resources*, *1*, pp.35-
609 53.

610 Uher, C. (2004). Thermal conductivity of metals. In *Thermal conductivity: theory,*
611 *properties, and applications* (pp. 21–91). Springer.

612 Wang, F., & Konietzky, H. (2019). Thermo-mechanical properties of granite at elevated
613 temperatures and numerical simulation of thermal cracking. *Rock Mechanics and*
614 *Rock Engineering*, *52*, 3737–3755.

615 Woods, J., Donaldson, C., White, R. S., Caudron, C., Brandsdóttir, B., Hudson, T. S., &
616 Ágústsdóttir, T. (2018). Long-period seismicity reveals magma pathways above a
617 laterally propagating dyke during the 2014–15 Bárðarbunga rifting event, Iceland.
618 *Earth and Planetary Science Letters*, *490*, 216–229.

619 Wright, T. J., Ebinger, C., Biggs, J., Ayele, A., Yirgu, G., Keir, D., & Stork, A. (2006).
620 Magma-maintained rift segmentation at continental rupture in the 2005 Afar dyking
621 episode. *Nature*, *442*(7100), 291-294.

622 Wright, T. J., Sigmundsson, F., Pagli, C., Belachew, M., Hamling, I. J., Brandsdóttir, B.,
623 Keir, D., Pedersen, R., Ayele, A., & Ebinger, C. (2012). Geophysical constraints on
624 the dynamics of spreading centres from rifting episodes on land. *Nature Geoscience*,
625 *5*(4), 242–250.

626 Zhang, S. (2022). Battling Gibbs phenomenon: On finite element approximations of
627 discontinuous solutions of PDEs. *Computers & Mathematics with Applications*, *122*,
628 35–47.

629

Supplementary Files

This is a list of supplementary files associated with this preprint. Click to download.

- dykethermomechfenicsx.py